Journal of Applied Polymer Science

Supermolecular Morphology of Polypropylene Filled with Nanosized Silica

Alois K. Schlarb,[1,2,3] Dwi N. Suwitaningsih,[1,3] Michael Kopnarski,[3,4] Gereon Niedner-Schatteburg[3,5]

[1]Composite Engineering, University of Kaiserslautern, Kaiserslautern, Germany
[2]Leibniz Institute for New Materials, Saarbrucken, Germany
[3]Research Center for Optics and Materials Sciences, University of Kaiserslautern, Kaiserslautern, Germany
[4]Institute for Surface and Thin Film Analysis, University of Kaiserslautern, Kaiserslautern, Germany
[5]Cluster Chemistry Group, Department of Chemistry, University of Kaiserslautern, Kaiserslautern, Germany
Correspondence to: A. K. Schlarb (E-mail: alois.schlarb@mv.uni-kl.de)

ABSTRACT: The supermolecular morphology of injection-molded SiO_2/polypropylene (PP) nanocomposites was investigated via thin sections analyzed under polarized light and the systematic development of an appropriate etching technique, which allowed the study of the supermolecular morphologies with light microscopy (LM) and high-resolution field emission scanning electron microscopy (FESEM). In parallel, information regarding the dispersion, distribution state, and morphology of SiO_2 particles was investigated via transmission electron microscopy (TEM) and scanning electron microscopy (SEM) of the ion-polished and fractured surfaces of SiO_2-filled PP. The TEM/SEM results demonstrated an almost homogeneous dispersion and distribution of SiO_2 particle agglomerates in the PP matrix. With polarized transmitting LM, reflecting LM, and FESEM, the spherulitic structure of the nanocomposites could be visualized to obtain information on the nanoparticle influence on the crystallization and structural behavior. The size and size distribution of the spherulites analyzed with transmitting light (thin sections) and reflecting light (etched specimens) showed an excellent correlation. With increasing filler loading, the mean size of the spherulites decrease as did the degree of crystallinity. This was a clear indication that the particles acted as nucleation agents and, on the other hand, hindered the arrangement of the molecules during the crystallization. As a result, the particles were most likely located in three areas: the center of the spherulites, the areas between the highly crystalline branches, and the spherulite boundaries. © 2013 Wiley Periodicals, Inc. J. Appl. Polym. Sci. **2014**, *131*, 39655.

KEYWORDS: composites; microscopy; morphology; polyolefins; thermoplastics

Received 2 February 2013; accepted 12 June 2013
DOI: 10.1002/app.39655

INTRODUCTION

It is known that physical properties and thus the application characteristics of polymers are highly dependent on their morphological structure. The morphological formation and morphology of semicrystalline thermoplastics and at least their structure–property relationships have been studied extensively over the last decades.[1–7] However, with regard to a new class of materials, the so-called nanocomposites, that have attracted great interest from academia and industry in recent years, there is a lack of knowledge in regard to the effects of nanofillers on the morphology of the resulting composites and on the relationship between the morphology and the properties. Nanocomposites show remarkable property improvements compared to virgin polymers; moreover, this occurs at very low filler loadings when compared to conventional microcomposites.[8] According to ref. 9, multiwalled carbon nanotubes influence the viscoelastic properties of polypropylene (PP) because of nucleation, which reduces the spherulite size. The same effect was observed for polyamide 66 reinforced with TiO_2 nanoparticles with sizes of 21 and 300 nm.[10] Yang et al[11] attributed the improved creep behavior of nanoparticle-reinforced polyamide to the mobility interference of the macromolecules caused by the nanoparticles in the amorphous areas of the polymer. However, evidence of the level of morphology could not be rendered. The key question in regard to this is the preferential location of nanosized particles in semicrystalline thermoplastic materials. As a first step, in this study, we investigated the microstructure of PP containing different loads of nano-SiO_2 (0, 1, and 4 vol %).

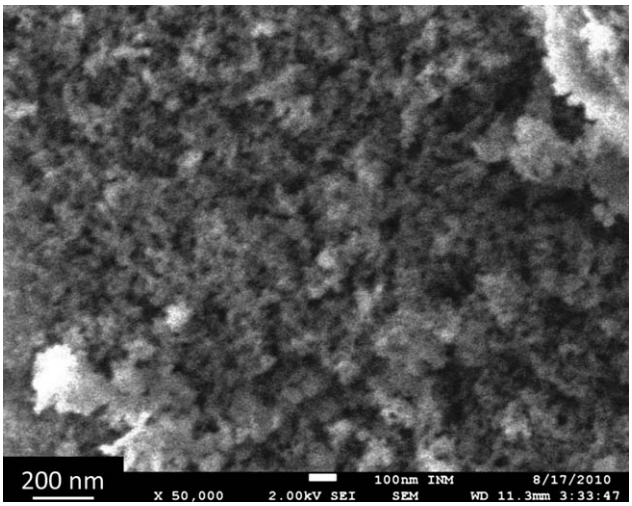

Figure 1. Initial agglomerated powder of SiO_2 (SEM image).

EXPERIMENTAL

Materials

PP granules (PP HD120 MO, Borealis GmbH) were used as a polymer matrix for all of the nanocomposites prepared in this study. SiO_2 ceramic nanoparticles (Aerosil R8200, Evonik Degussa GmbH) were used as inorganic nanofillers. The nanoparticles were provided in powder form and consisted of agglomerates about 200 nm in diameter (Figure 1).

The primary particle size given by the manufacturer was 12 nm. Three loading levels of SiO_2 nanoparticles, 0.0, 1.0, and 4.0 vol %, were prepared to systematically examine the influence of the SiO_2 nanoparticles on the crystallization behavior and thus the resulting supermolecular structure of the polymer. The nanocompounds were prepared via an optimized twin-screw extrusion. First, PP nanocomposites with a 5 vol % content of SiO_2 particles were extruded under a screw speed of 160 rpm. The temperatures were set from 190°C near the hopper to 210°C at the die. The obtained PP/SiO_2 nanocomposites were then diluted to 1 and 4 vol % SiO_2 particle content with the same extruder under identical conditions. Then neat PP and PP/SiO_2 nanocomposites were injection-molded into 70 × 70 × 4 mm^3 sheets. The process guarantied the best deagglomeration and homogeneous distribution of the SiO_2 nanofillers in the PP matrix. The procedure was described by Knör at al[12] in detail, and the possible effect and mechanisms of the procedure were discussed by Schlarb.[13]

Preparation of the Specimens

To study the morphology of bulk-crystallized samples, we cut the center part of the injection-molded sheet into rectangular cuboids, according to Figure 2. The rough cross section perpendicular to the mold surface imposed by the cutting tool was then removed by a microtome to yield a smooth surface. For surface preparation, microtomy was chosen over the more rigorous, time-consuming mechanical polishing method to eliminate noncharacteristic features of the specimen before surface modification.

To compare the morphologies between the etched and nonetched surfaces, we carried out a microscopy analysis on a 10-μm thin section of each specimen before etching. The thin section was cut out of the cross section of every specimen with a Hyrax M 25 rotation microtome equipped with a steel blade. The section was then immersed in oil between two objective glasses for LM investigation.

Ultrathin sections for transmission electron microscopy (TEM) analysis were prepared by wet room temperature ultramicrotomy with a Reichert Ultracut E Ultramicrotome equipped with a 35° diamond knife for ultrathin sections. The thickness of the sections used in the following TEM observations was about 50 nm as it was determined based on the section color during the cutting procedure. After it was cut with the microtome, the remaining bulk specimen was further cleaned with distilled water before etching.

The permanganic etchant was prepared according to a procedure described by Bassett and Olley[14] and Shahin et al.[15] For this experiment, a solution with a 0.7% w/v permanganate solution was prepared by the addition of 1.47 g of potassium permanganate crystals to 210 mL of a mixture of 2:1 by volume 98% sulfuric acid and 85% phosphoric acid; this mixture had previously been cooled down to room temperature. The mixture

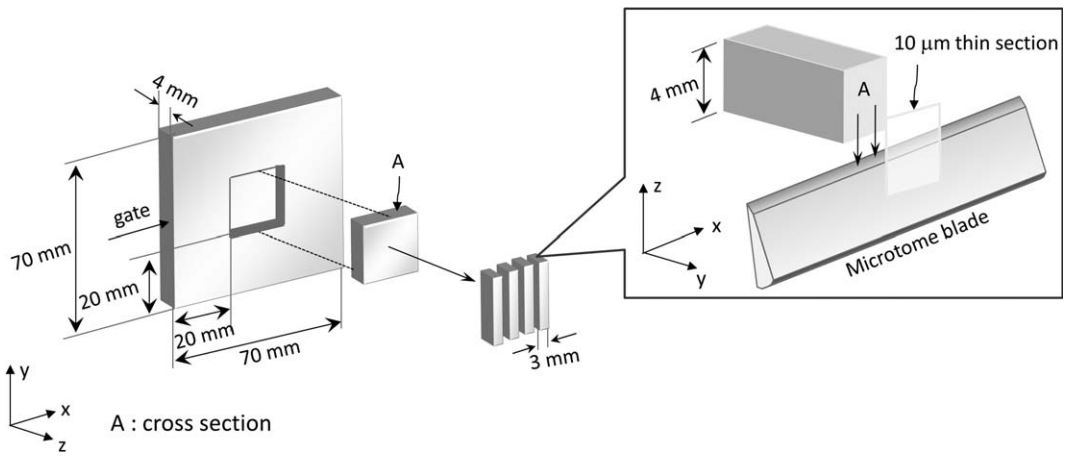

Figure 2. Preparation of the specimens.

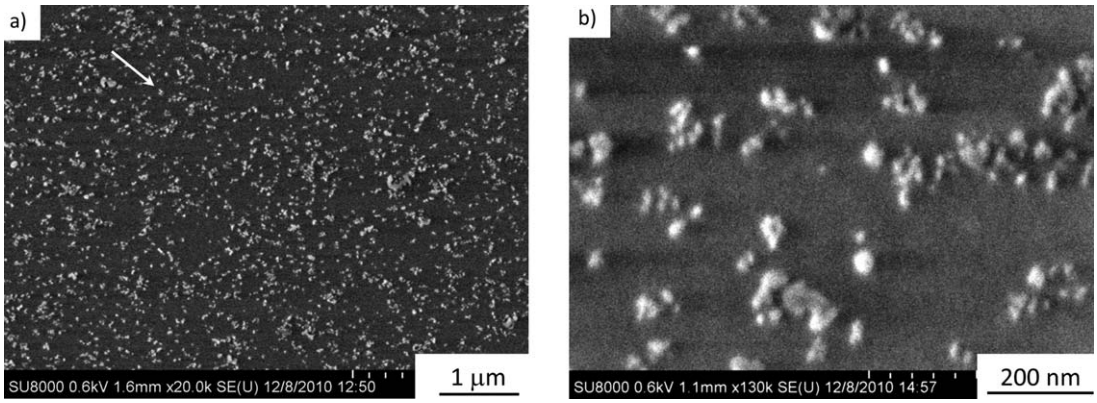

Figure 3. (a) High-resolution SEM images of an ion-polished sample of PP filled with 4 vol % SiO_2 nanoparticles and (b) a magnified image of the marked area.

was then stirred with a magnetic stirrer until the permanganate crystals were thoroughly dissolved (ca. 30 min) to give a concentrated deep green solution. The specimens were then introduced to the etchant and stirred rigorously for 18 h at room temperature and then for 6 h at 60°C.

Near the end of etching period, a washing solution was prepared by the mixing of 2:7 by volume of concentrated sulfuric acid and water, and the solution was allowed to cool to room temperature. To 10 parts volume of this solution, 1 part volume of 30% hydrogen peroxide was added, and the mixture was stirred. The resulting solution was then cooled down with an ice bath.

At the end of the etching period, the etchant and the specimens were poured into the cold washing solution and were shaken for 3 min to yield a clear liquid, and the specimens were further washed with distilled water and finally with methanol.

The ion-polished surfaces were prepared with a Hitachi E-3500 cross-sectional polisher operating with a wide argon-ion beam, which cut the material and yielded a fine cross section with mirrorlike finish without any structural damage. The polished sample was characterized with a high-resolution scanning electron microscope (Hitachi SU 8000) operating with a 0.6-kV acceleration voltage and a working distance of 2 mm.

Microscopic Investigations

A polarizing light microscope (Zeiss Axio Imager A.1M) equipped with circular differential interference contrast (c-DIC) feature was used to observe the morphology of the etched specimens before further analysis with scanning electron microscopy (SEM) and TEM.

A combination of a focused ion beam/field emission scanning electron microscope (FEI Altura 875 Dualbeam), operating with a 5-kV acceleration voltage, and a secondary electron detector, with a working distance of 5 mm, was used to observe the supermolecular structure of the samples. All of the samples were sputter-coated with 10 nm of gold palladium before the SEM analysis.

TEM of PP filled with different SiO_2 contents was done to analyze the distribution of the nanoparticles within the PP matrix and to characterize the used nanoparticles by themselves, their dimensions, and their crystal structure. The investigations were carried out with a JEOL JEM 2011 TEM instrument with an LaB6 cathode. Different zones of different injection-molded specimens of the same batch were analyzed, and the images that are presented are the most representative.

Thermal Analysis

The thermal properties and the melting behavior of the samples were determined by differential scanning calorimetry (DSC; Mettler-Toledo). The samples were cooled to 0°C, heated to 200°C, and cooled down to 0°C at a rate of 10 C/min. The cycle was repeated for each sample to erase the initial thermal and processing history and to obtain the representative thermal properties. The DSC curves depicted in this article were taken from the second run. The degree of crystallinity (X_c) was calculated with eq. (1):

$$X_c = \frac{\Delta H_s}{\Delta H_k} 100 \qquad [\%] \tag{1}$$

where ΔH_s is the measured enthalpy of fusion and ΔH_k is 209 J/g (literature data for the enthalpy of fusion of 100 % crystalline polypropylene).

RESULTS AND DISCUSSION

Small-Scale Dispersion and Nature of the Used SiO_2

Figure 3(a) depicts the high-resolution SEM of an ion-polished sample where the nanoparticles were uniformly distributed in the PP matrix. The high magnification of the marked area [Figure 3(b)] reveals agglomerates in the size range of 35–140 nm and the primary nanoparticles.

The TEM images [Figure 4 (a,b)] showed that the nanoparticles were mainly present in the form of small groups. These groups were practically uniformly distributed within the polymer matrix.

Fractured specimens were prepared for the pure PP as well as for all concentrations of filled PP to reveal the dispersion of the nanoparticles in the matrix. The samples were each frozen in liquid nitrogen before they were fractured to retain their dispersion behavior in the matrix and to minimize nonstructural artifacts due to plastic deformation. Figure 5 reveals a

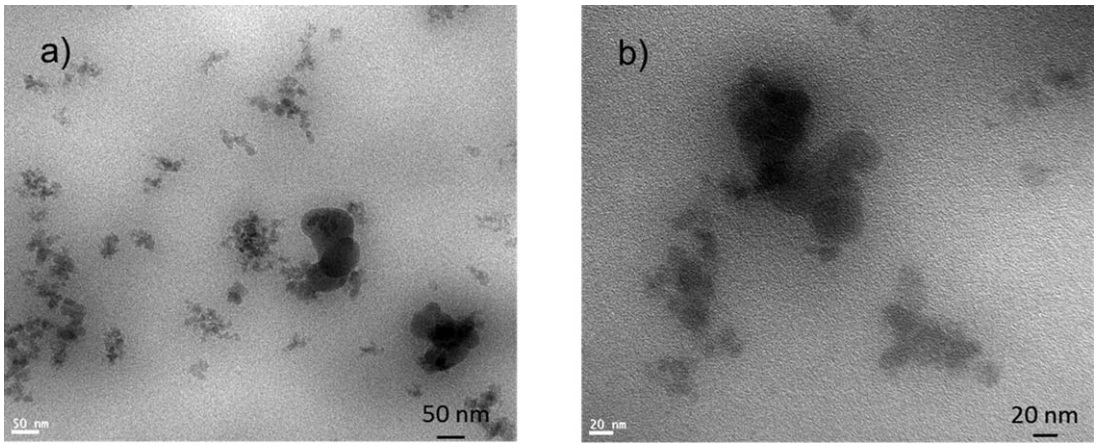

Figure 4. TEM images taken from some regions of PP filled with 1 vol % SiO_2 nanoparticles: a representative example.

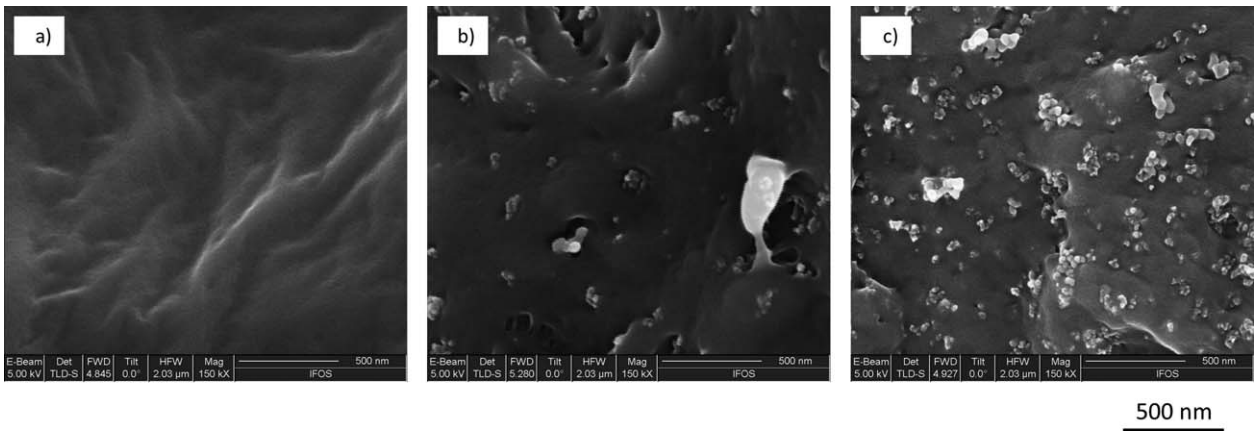

Figure 5. SEM images of the fractured surfaces of (a) pure PP, (b) PP filled with 1 vol % SiO_2, and (c) PP filled with 4 vol % SiO_2.

homogeneous dispersion of nanoparticles for various concentration ratios of SiO_2-filled PP. This finding signified an optimum deagglomeration that seemingly originated from the multistep compounding process.

Supermolecular Morphology

Microscopy. The spherulitic structures of the etched surfaces of the pure PP and PP reinforced with 1.0 and 4.0 vol % SiO_2 nanoparticles, respectively, were characterized by LM (Figure 6). The images revealed a homogeneous polyhedral spherulitic morphology with sharp boundaries, each made of fibrils radiating from the center to the circumference, which adjoined with the border with the neighboring spherulites. From visual observation, the SiO_2-filled PP seemed to have spherulites in the same order of magnitude as pure PP without any obvious shape changes due to nanoparticles. Other than SEM or TEM,

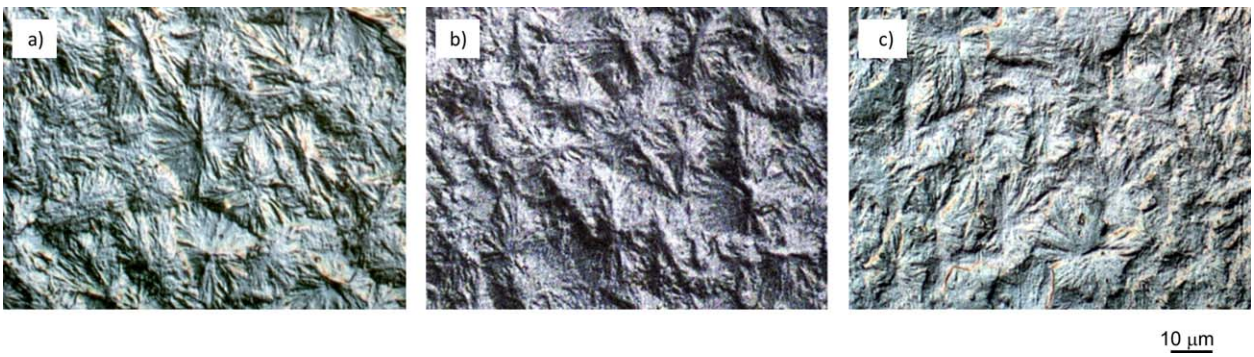

Figure 6. LM images of the spherulitic structure of (a) pure PP, (b) PP filled with 1 vol % SiO_2, and (c) PP filled with 4 vol % SiO_2. [Color figure can be viewed in the online issue, which is available at wileyonlinelibrary.com.]

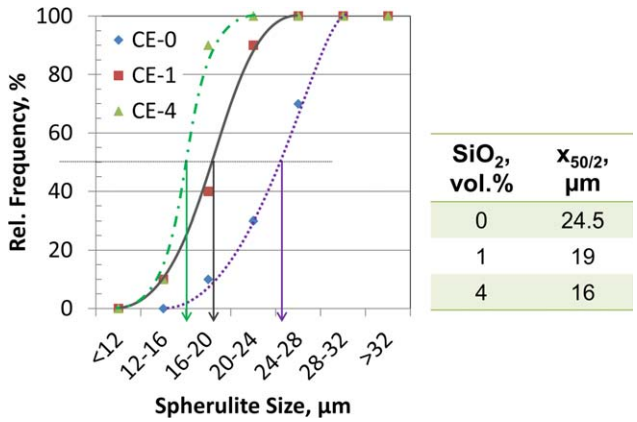

SiO_2, vol.%	$x_{50/2}$, µm
0	24.5
1	19
4	16

Figure 7. Polarized LM images of the thin sections of (a) pure PP, (b) PP filled with 1 vol % SiO_2, and (c) PP filled with 4 vol % of SiO_2. [Color figure can be viewed in the online issue, which is available at wileyonlinelibrary.com.]

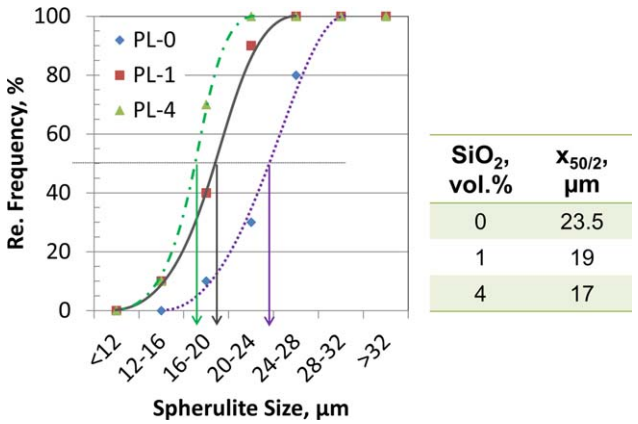

SiO_2, vol.%	$x_{50/2}$, µm
0	23.5
1	19
4	17

Figure 9. Cumulated relative frequency (Rel. Frequency) as a function of the spherulitic diameter for three different SiO_2 nanoparticle loadings in chemically etched samples (CE). [Color figure can be viewed in the online issue, which is available at wileyonlinelibrary.com.]

individual nanoparticles or nanoparticle agglomerates were not observable by LM at the resolution we used.

The qualitative analysis on the spherulite size was carried out by application of the ASTM standard for grain size determination.[16] Figure 6 represents the relative frequency of the spherulitic diameters of the nanocomposites up to 32 μm divided into five categories each with 4-μm increments. It was obvious that the median of the diameter distribution in two dimensions $X_{50/2}$ shifted to a lower diameter range with increasing SiO_2 content. The size of the neat PP spherulites (CE-0) peaked at 24.5 μm, whereas the values of those filled with 1 (CE-1) and 4 vol % SiO_2 (CE-4) peaked at 19 and 16 μm, respectively. It can be said that the addition of SiO_2 nanoparticles leads to a decrease in the spherulite size. This had no influence on the spherulitic shape of the PP matrix. We assume that the particles acted as a nucleating agent, which accelerated the crystallization process and led to smaller spherulites. To verify this suggestion, thermal analysis was carried out (see later discussion).

The analysis of the supermolecular structure of the nonetched samples was carried out with thin sections by LM under polarized light. The spherulites in this case appeared with birefringence in a Maltese cross pattern (Figure 8).

The spherulite sizes were determined by Heyn's method for grain size measurement. This revealed a shift in the median $X_{50/2}$ (Figure 9) in parallel to the trend observed in Figure 7. In both cases, the spherulitic diameter decreased with increasing SiO_2 filler content. Although the values of both methods were not absolutely identical, the range of the relative frequency peak for each specimen was almost the same. The slight difference may have arisen from the fact that the borders between spherulites were not as apparent as those in the etched surface. Apart from that, the morphology revealed by permanganic etching and viewed with c-DIC fell in the same size range as those observed in a thin section of the bulk material and viewed with transmitted polarized light. Therefore, we are certain that permanganic etching did not alter the morphology of the specimens.

To investigate the effect of the SiO_2 nanoparticles on the supermolecular structure of the PP matrix, the etched samples were characterized by field emission scanning electron microscopy (Figure 10). This illustrated the dispersion of nanoparticles in relation to the spherulitic morphology. At the used magnification, it was evident that the fibrils resembled branches with sizes ranging from 100 to 650 nm across. These fibrils appeared to be bundles of lamellae, as the latter have been reported to

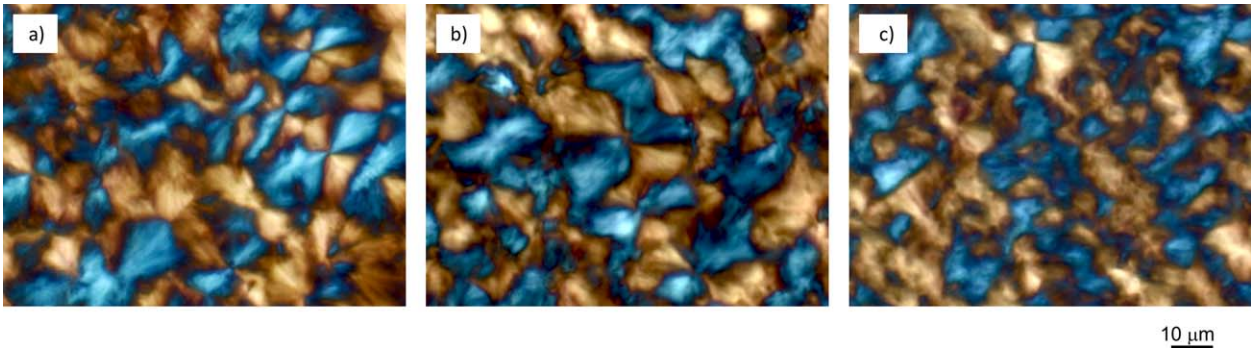

Figure 8. Cumulated relative frequency (Re. Frequency) as a function of the spherulitic diameter of three different SiO_2 nanoparticle loadings in thin sections (PL, polarized light). [Color figure can be viewed in the online issue, which is available at wileyonlinelibrary.com.]

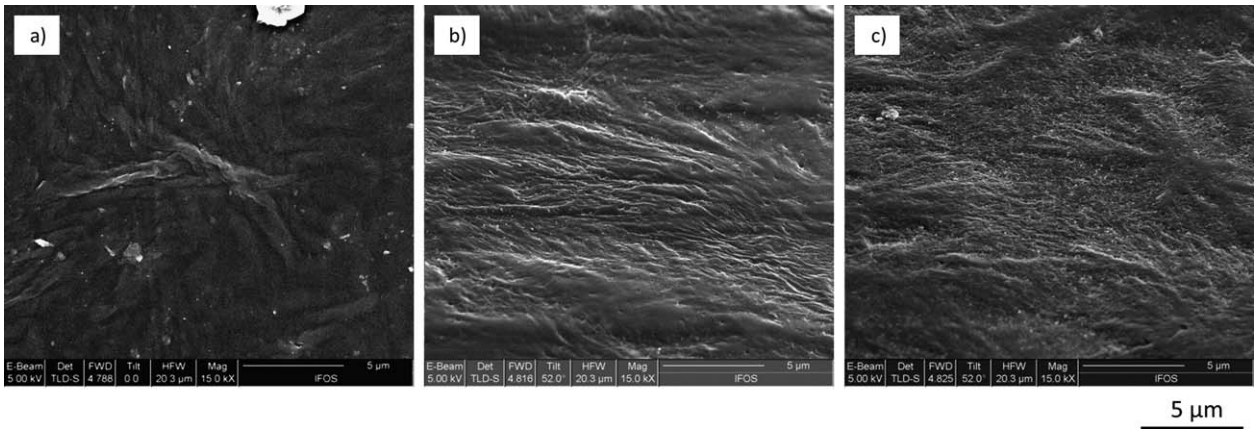

Figure 10. SEM images of the spherulitic structures of (a) pure PP, (b) PP filled with 1 vol % SiO_2, and (c) PP filled with 4 vol % SiO_2.

Figure 11. Composite image of the 4 vol % SiO_2-filled PP showing the distribution of SiO_2 nanoparticles among the spherulites.

have the thicknesses in the range 12–14 nm.[17,18] It is notable that the exposed nanoparticles were seemingly dispersed between these branches and at the boundary between the spherulites.

The nanoparticle distribution became further apparent through a composite image acquired by the stitching of 25 SEM images of 4 vol % SiO_2-filled PP at 50,000× magnification (Figure 11). To emphasize the topography of the spherulitic structure, the sample was tilted at 52°.

In relation to the spherulite, the nanoparticles are seen to be more dispersed in low lying areas between the branches and at the border of spherulites. Further spherulites are possibly lying underneath the high crystalline areas. The concave points are attributed to the areas of low crystallinity which are more prone

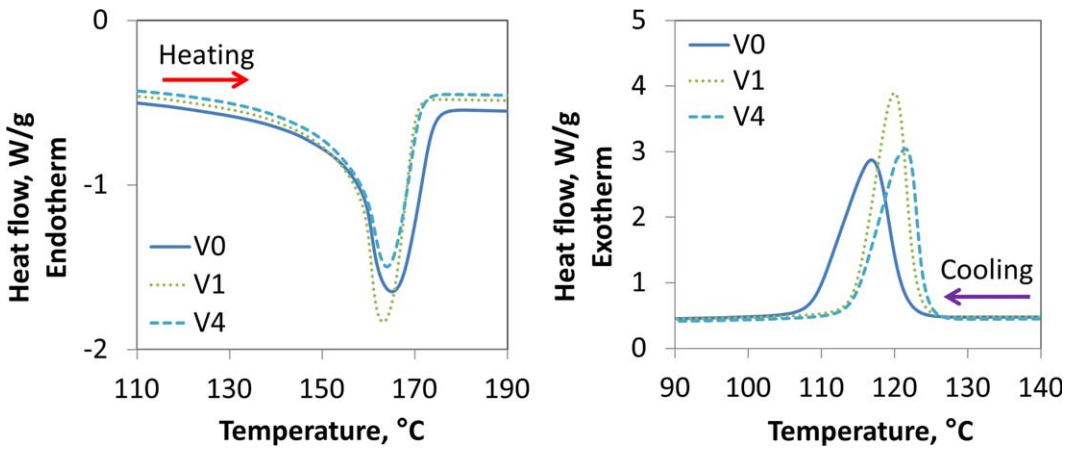

Figure 12. DSC heating and cooling curves at 10 K/min for pure PP (V0) and PP filled with (V1) 1 and (V4) 4 vol % SiO_2 nanoparticles. [Color figure can be viewed in the online issue, which is available at wileyonlinelibrary.com.]

Table I. Thermal Properties of the Pure PP and Reinforced PP Samples with Different SiO_2 Loadings

Sample	T_c (°C)	ΔH_c (J/g)	T_m (°C)	ΔH_m (J/g)	X_c (%)
Neat PP	116.8	115.3	165.1	126.8	60.7
PP + 1 vol % SiO_2	120.0	117.4	163.2	125.9	60.2
PP + 4 vol % SiO_2	121.5	103.3	163.9	117.4	56.2

T_c = crystallization temperature, ΔH_c = heat of crystallization, T_m = melting temperature, ΔH_m = heat of fusion, X_c = degree of crystallinity.

to acid attack compared to the spherulite center and lamellae bundle.

Thermal Analysis. The melting behavior of the pure and SiO_2-filled PP crystallized under nonisothermal conditions was analyzed with DSC (Figure 12). The peak of the melting curve hardly changed with the addition of SiO_2 nanoparticles. It is well known that isotactic polypropylene (iPP) has four different crystal forms: a monoclinic α phase, a trigonal β phase, an orthorhombic γ phase, and a smectic phase.[19–21] In the crystallization of conventional iPP, essentially, the α phase is formed and is accompanied by a trigonal β phase; the former is signified by melting at 165°C, whereas the latter melts at 154°C.[22] The pure PP and all of the nanocomposites exhibited a characteristic α-phase crystal melting temperature of about 164°C. The presence of SiO_2 particles thus had little influence on the melting behavior of the PP matrix.

Upon cooling from the melt, crystallization took place at a higher temperature with increased SiO_2 loading. The neat PP exhibited the crystalline peak at 116.7°C. With the addition of 1 and 4 vol % SiO_2 nanoparticles, the value increased to 120 and 121.5°C, respectively; this suggested an earlier start of crystallization at a given cooling rate. This result substantiated our assumption that the SiO_2 nanoparticles acted as a nucleating agent during crystallization and agrees with refs. 23–25, which stated that most inorganic fillers can act as nucleating agents for iPP and increase the crystallization temperature (Table I).

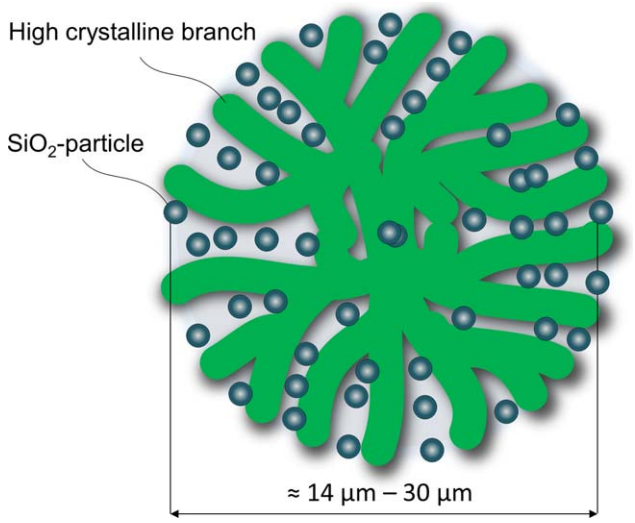

Figure 13. Preferential location of the SiO_2 nanoparticles in a PP spherulite: a skeleton sketch. [Color figure can be viewed in the online issue, which is available at wileyonlinelibrary.com.]

CONCLUSIONS

The incorporation of nanosized SiO_2 into a PP homopolymer decreased the size of the spherulites of the resulting nanocomposites. The spherulitic diameters of the pure and SiO_2-reinforced PP nanocomposites were in the range 14–30 μm, and the peak frequency of the spherulite size shifted to a lower value with increasing SiO_2 content. No considerable change in the shape of spherulites was examined by LM with c-DIC on the chemically etched specimens or by transmitted polarized light of the corresponding thin sections. As a result, we can state that the use of chemical etching did not affect the morphology. The SEM analysis of the etched samples also revealed that the nanoparticles were more dispersed at the area of lower crystallinity. The DSC results shows that the SiO_2 nanoparticles in parallel decreased the degree of crystallinity of the PP matrix and the size of the resulting spherulites. This is a clear indication that the particles acted as nucleation agents and, on the other hand, hindered the arrangement of the molecules during crystallization. As a result, the particles were most likely located in three areas: the center of the spherulites, the areas between the crystalline branches, and the spherulite boundaries (Figure 13).

ACKNOWLEDGMENTS

The authors thank the Carl Zeiss Foundation for its financial support of this work. They also thank L. Lin (Chair of Composite Engineering, Kaiserslautern, Germany) and V. Demchuk (Polymer Engineering, Hamburg-Harburg) for the compounding and injection molding of the nanocomposite specimens, B. Reuscher and A. Zeuner (Intitute for Surface and Thin Film Analysis, Kaiserslautern, Germany) for the high-resolution SEM images, M. Koch and Hettich (Leibniz Institute for New Materials, Saarbrucken, Germany) for the TEM pictures, S. Wolff (Nano Structuring Center, Kaiserslautern, Germany) for the preparation of the ion-polished specimens, R. Drumm (Leibniz Institute for New Materials, Saarbrucken, Germany) for DSC measurements, and Borealis and Evonik for providing the materials needed for this study.

REFERENCES

1. Keller, A. *Nature* **1952**, *169*, 913.
2. Keller, A. In Reports on Progress in Physics; Pedersen, C. I., Ed.; Institute of Physics and Physical Society: London, **1968**; p 623.
3. Kanig, G. Kolloid-Z. Z. *Polym.* **1973**, *251*, 782.
4. Ramesh, C.; Keller, A.; Eltrink, S. E. A. *Polymer* **1994**, *35*, 5293.
5. Varga, J.; Mudra, I.; Ehrenstein, G. W. *J. Appl. Polym. Sci.* **1999**, *10*, 2357.
6. Magill, J. H. *J. Mater. Sci.* **2001**, *36*, 3143.

7. Mandelkern, L. Crystallization of Polymers; Cambridge University Press: Cambridge, United Kingdom, **2002**.
8. Jog, J. In Optimization of Polymer Nanocomposite Properties; Mittal, V., Ed; Wiley-VCH: Weinheim, **2010**; Chapter *13*, p 279.
9. Ganß, M.; Satapathy, B. K.; Thunga, M.; Weidisch, R.; Poetschke, P.; Janke, A. *Macromol. Rapid Commun.* **2007**, *28*, 1624.
10. Yang, J.-L. Ph.D. Thesis, University of Kaiserslautern, **2006**.
11. Yang, J.-L.; Zhang, Z.; Schlarb, A. K.; Friedrich, K. *Polymer* **2006**, *47*, 6745.
12. Knör, N.; Haupert, F.; Schlarb, A. K. Nanoverbundwerkstoffe—Eine Neue Materialklasse mit Verbesserter Steifigkeits-/Zähigkeitsrelation; IVW-Verlag: Kaiserslautern, Germany, **2008**.
13. Schlarb, A. K. Perspektiven der Kunststofftechnik im Zusammenwirken von Werkstoff und Verarbeitung; RWTH Aachen: Aachen, Germany, **2008**.
14. Bassett, D. C.; Olley, R. H. *Polymer* **1984**, *25*, 935.
15. Shahin, M. M.; Olley, R. H.; Blissett, M. J. *J. Polym. Sci. Part B: Polym. Phys.* **1999**, *37*, 2279.
16. In Book of Standards; ASTM International: West Conshohocken, PA; Vol. 03.01; ASTM E 112-10.
17. Włochowicz, A.; Eder, M. *Polymer* **1984**, *25*, 1268.
18. Spieckermann, F.; Wilhelm, H.; Kerber, M.; Schafler, E.; Polt, G.; Bernstorff, S.; Addiego, F.; Zehetbauer, M. *Polymer* **2010**, *51*, 4195.
19. Varga, J. *J. Mater. Sci.* **1992**, *27*, 2557.
20. Lotz, B.; Wittmann, J. C.; Lovinger, A. *J. Polymer* **1996**, *37*, 4979.
21. Varga, J. *J. Macromol. Sci. Part B: Phys.* **2002**, *41*, 1121.
22. Zhang, Y.-F. *J. Polym. Sci. Part B: Polym. Phys.* **2008**, *46*, 911.
23. Chan, C. M.; Wu, J. S.; Li, J. X.; Cheung, Y. K. *Polymer* **2002**, *43*, 2981.
24. Qian, J. S.; He, P. S.; Nie, K. J. *J. Appl. Polym. Sci.* **2004**, *91*, 1013.
25. Bikiaris, D. N.; Papageorgiou, G. Z.; Pavlidou, E.; Vouroutzis, N.; Palatzoglou, P.; Karayannidis, G. P. *J. Appl. Polym. Sci.* **2006**, *100*, 2684.